MINISTER OF EDUCATION AND TRAINING

VIETNAM ACADEMY OF SCIENCE AND TECHLONOGY

GRADUATE UNIVERSITY OF SCIENCE AND TECHLONOGY

Nguyen Thi Hanh

RESEARCH ON THE PREPARATION OF NANOMATERIALS FOR THE ADSORPTION OF TOXIC GASES AND FIRE-RETARDANT ADDITIVES IN THE HIGH-DENSITY POLYETHYLENE COMPOSITE

SUMMARY OF DISSERTATION ON CHEMISTRY

Code: 9 44 01 13

Hanoi - 2023

The dissertation is completed at Graduate University of Science and Technology - Vietnam Academy of Science and Technology

Supervisors:

1. Supervisor 1: Prof. Dr. Nguyen Van Tuyen
2. Supervisor 2: Dr. Hoang Mai Ha

Referee 1: Prof. Dr. Do Quang Khang
Referee 2: Assoc. Prof. Dr. Nguyen Thi Thanh Chi
Referee 3: Assoc. Prof. Dr. Pham Anh Son

The dissertation has been examined by Examination Board of Graduate University of Science and Technology, Vietnam Academy of Science and Technology at 9 am on Oct 13th, 2023

The dissertation can be found at:

1. Library of Graduate University of Science and Technology
2. National Library of Vietnam

INTRODUCTION

1. Rationale of the thesis

Unwanted fires cause serious losses of life and property all over the world. The majority of casualties are due to inhalation of smoke and toxic gases. Therefore, it is necessary to study on and fabricate of materials capable of reducing toxic gases, contributing to the protection of rescuers and people trapped in the fire incidents.

Many types of flame-retardants have been studied and used, however, it is necessary to pay attention to the risk of flame-retardants on the users' health. Nowadays, nano flame retardants are considered to be more environmentally friendly. Nano fillers help the base materials to be fire-resistant while maintaining and/or improving physical-mechanical properties such as strength, lightness, thinness.

From above practical and scientific basis, we have chosen the topic ***"Research on the preparation of nano materials for the adsorption of toxic gases and fire-retardant additives in the HDPE composite"***.

2. Aims of the thesis

- Study on the preparation of several inorganic oxides and salts including Fe_3O_4, ZnO, $CaCO_3$ and $MgCO_3$ that might be capable of reducing the toxic gases in fire incidents.
- Study on the synthesis of nano zinc borate that might be used as a flame - retardant additive in polymer matrices.

3. Scope of the thesis

- Research on the synthesis of Fe_3O_4, ZnO, $CaCO_3$ and $MgCO_3$ nanomaterials by suitable methods.

- Evaluation of the adsorption capacity of the obtained nanomaterials for some toxic gases commonly encountered in fire incidents such as NO_2, SO_2, HCN, and CO.

- Research on the synthesis of nano zinc borate (nZB) for application as flame - retardant additives.
- Evaluation on the synergistic flame - retardance of nZB in combination with other flame retardants in HDPE composites.

CHAPTER 1. LITERATURE REVIEW

1.1. Overviews of fire chemistry

Combustion processes consist of three basic elements including fuel, oxygen and heat. Recently, a fourth necessary element has been added, that is a chain reaction in the combustion of fuel accompanied by the infinite formation of HO*, H*, R* free radicals. From there, the principle of fire prevention and fighting practice is to eliminate one of the elements of heat, fuel, oxygen, or break the chain reaction circuit. In addition to smoke and acute toxic gases such as CO, HCN, SO_2, NO_2, there are also carcinogenic substances emitted from fires.

1.2. Overviews of nanomaterials used in the removal of smoke and toxic gases

Nanomaterials have been studied, manufactured and applied widely. Nano inorganic materials have been intensively studied to treat pollutants, especially in the removal of heavy metals in water and wastewater. Metal oxide nanoparticles exhibit good adsorption capacity for toxic substances at room temperature as well as at high temperature. It has also now been clearly demonstrated that nano oxides have unique surface properties in comparison to microcrystalline and bulk oxides.

1.3. Overviews of fire-retardants and nano zinc borate

Flame retardant (FR) materials can be classified according to the mechanism of fire resistance or by chemical composition. According to chemical composition, FRs are usually classified into groups of halogen FRs, inorganic FRs, organic FRs, swelling FRs and nano filler FRs.

Zinc borate is often used as an additive or charring agent in polymers, rubber and coatings. It does not emit toxic or corrosive substances during combustion. Some types of zinc borate have high decomposition temperatures, which offer significant advantages in combination with polymers requiring high fabrication temperature. Zinc borate can reduce heat release rate and smoke formation, especially in polymers containing metal hydroxides. The main effect of zinc borate is to promote the formation of a hard char like ceramic. This deposit prevents drip burning, delays oxidative pyrolysis, and protects the polymer underneath.

However, zinc borate also has some disadvantages. It is need to use a large amount to achieve high effects and difficult to disperse uniformly in the polymer with coarse sizes.

CHAPTER 2. MATERIALS AND METHODOLOGY

2.1. Chemicals, apparatus

2.2. Preparation of nano materials for toxic gases adsorption

The nFe_3O_4 was prepared by co-precipitation using $FeCl_2.4H_2O$ and $FeCl_3.6H_2O$ with Fe^{2+}/Fe^{3+} molar ratio of ½ in the atmosphere of N_2 gas. The nZnO and nZnO-SLS were prepared by precipitation using $Zn(OH)_2$ and NaOH, SLS was used as a surfactant. The n$CaCO_3$ was precipitated from solutions of Na_2CO_3 and $CaCl_2$, the surfactants used included CTAB, EDTA, PEG, PVA, and SLS. The n$MgCO_3$ was synthesized by precipitation or hydrothermal methods. The precursors were $MgCl_2$ or $Mg(CH_3COO)_2$ salt and $NaHCO_3$, the surfactant used was Tw80.

2.3. Preparation of nano zinc borate as a fire-retardant

The nZB was synthesized from solutions of $ZnSO_4$ salt and the mixed solutions of H_3BO_3 acid and NaOH at different pH. The mixtures were heated at varied temperatures. The effects of pH, temperature and

surfactants on the formation of nZB were investigated.

The flame-retardant HDPE were fabricated by melt mixing method at 175 ^{o}C and hot pressed into flat sheets of 3 mm thick. The samples were stabilized for at least 24 hours prior to characterization.

2.4. Characterization and investigation on the application potentials of the nanomaterials

The synthesized nanomaterials were characterized by XRD, FT-IR, SEM, TGA-DTA methods. The porous structure and specific surface area of adsorbents were investigated in N_2 atmosphere using BET theory.

The adsorption tests of nFe_3O_4, nZnO, $nMgCO_3$, and $nCaCO_3$ were carried out at ambient temperature in a fixed-bed reactor. The adsorbates included NO_2 and SO_2 gases. Besides, the nZnO oxides were investigated for the adsorption of HCN gas. The adsorption of CO gas was preliminarily tested on the $nMgCO_3$. The adsorption capacities were determined using gravimetric method. Concentrations of influent gases were analyzed on KIMO KIGAZ 300 and ToxiRAE II monitors. After adsorption, adsorbents were analyzed again by FT-IR, XRD, and SEM-EDX methods to deduce their adsorption abilities.

The HDPE nanocomposites were tested for flame-retardancies including LOI, UL94-V, and mechanical properties including tension strength, elongation at break and unnotched Izod impact strength .

CHAPTER 3. RESULTS AND DISCUSSION

3.1. Characteristics of nanomaterials for toxic gases adsorption

3.1.1 Characteristics of nFe_3O_4

The XRD and CO-TPR results (*Fig. 3.1*) revealed that as-synthesis material was monophase Fe_3O_4. On the FT-IR spectrum, the intense peak at wavenumber of approximately 583 cm^{-1} was assigned to the valence vibration of Fe-O which is usually observed in AB_2X_4 spinel structures.

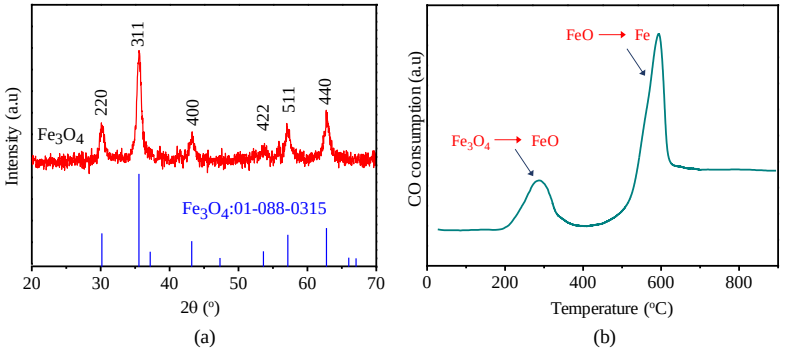

Fig. 3.1. (a) XRD pattern, (b) CO-TPR profile of nFe_3O_4

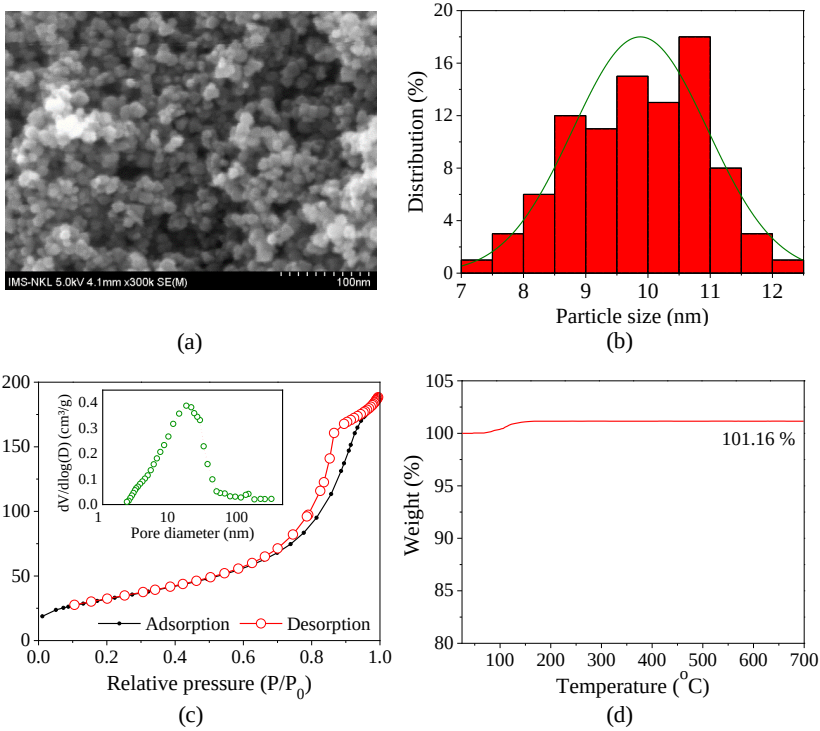

Fig. 3.3. (a) SEM, (b) Particle-size distribution, (c) Adsorption/desorption isotherm of N_2 and pore-size distribution, (d) TGA of nFe_3O_4

The SEM (*Fig. 3.3a*) and TEM images showed that the nFe_3O_4 particles agglomerated to form porous structures. The BET specific

surface area (*Fig. 3.3c*) of nFe_3O_4 was approximately 116 m^2/g, the average of pore diameters was of 10.6 nm and the adsorption cumulative volume of pores was 0.3 cm^3/g.

3.1.2 Characteristics of nZnO

The diffraction peaks on XRD patterns (*Fig. 3.5a*) of the nZnO and nZnO-SLS matched well with monophase structure of hexagonal zinc oxide crystal (JCPDS 01-076-0704). No diffraction peaks associated with other zinc compounds were observed. Sharp diffraction peaks illustrated the high crystallinity of as-prepared nZnO and nZnO-SLS. The weight percentage of pristine zinc oxide in the nZnO and nZnO-SLS samples deduced from the TGA-DTA data were of 98.9% and 94.5% respectively (*Fig. 3.5b*).

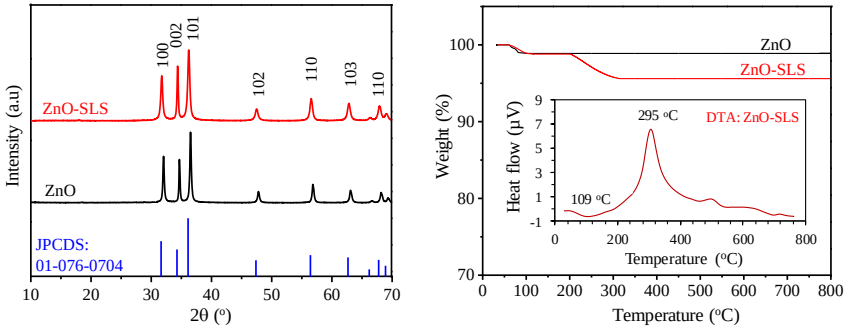

(a) (b)

Fig. 3.5. (a) XRD pattern and (b) TGA/DTA of nZnO and nZnO-SLS

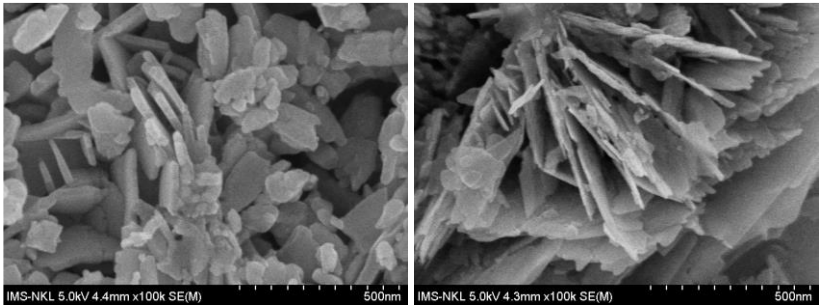

(a) (b)

Fig. 3.6. SEM images of (a) nZnO and (b) nZnO-SLS samples

In the SEM images (*Fig. 3.6*), the nZnO and nZnO-SLS samples were nanoplate shaped particles. The nZnO was about 25 - 30 nm thick and 100 - 200 nm wide. In the presence of SLS surfactant, the nZnO-SLS was significantly thinner and wider (15 - 20 nm in thickness and 400 - 600 nm in width).

3.1.3 Characteristics of nCaCO₃

The XRD patterns of the precipitates obtained from the reaction of $CaCl_2$ and Na_2CO_3 salts were in accordance with the file JCPDS 01-071-3699 of $CaCO_3$ in calcite form. The surfactants had no obvious effect on the crystalline phase but remarkably changed the shape of nanoparticles. With SLS, the $CaCO_3$-SLS particles were nanoplates of 25 - 50 nm thick and over 100 nm wide.

3.1.4 Characteristics of nMgCO₃

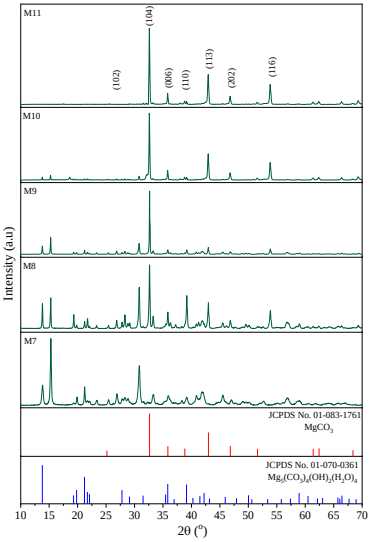

Fig. 3.14. XRD patterns of $MgCO_3$ samples prepared by hydrothermal method from $Mg(CH_3COO)_2$

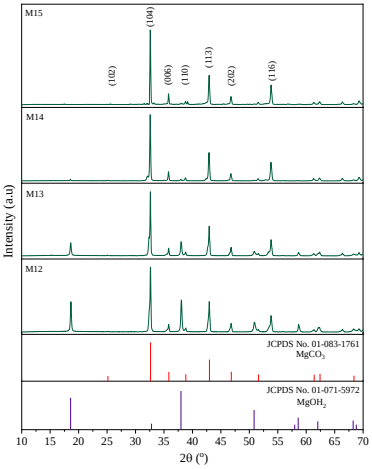

Fig. 3.15. XRD patterns of $MgCO_3$ samples prepared by hydrothermal method from $MgCl_2$

The XRD results indicated that the HCO_3^- concentration and hydrothermal time had an important role in the formation of single-phase $MgCO_3$. The anions of Mg^{2+} salt could affect the forms of intermediate products but not the crystal phase of the final product. The suitable reaction conditions to obtain single-phase $MgCO_3$ were the molar ratio of HCO_3^-: Mg^{2+} of 1.2 : 1, hydrothermal time about 24 hours.

The SEM images (*Fig. 3.18*) showed that the $nMgCO_3$ were heterogeneous in shape and size. Meanwhile, the $nMgCO_3$-Tw80 had a well-defined hydrangea-like shape with diameters ranged between 5 and 10 µm. The spherical flowers were interconnected by ultra-thin nanoplates of 10 - 15 nm in thickness forming the pores shaped of a triangular or tetragonal pyramid.

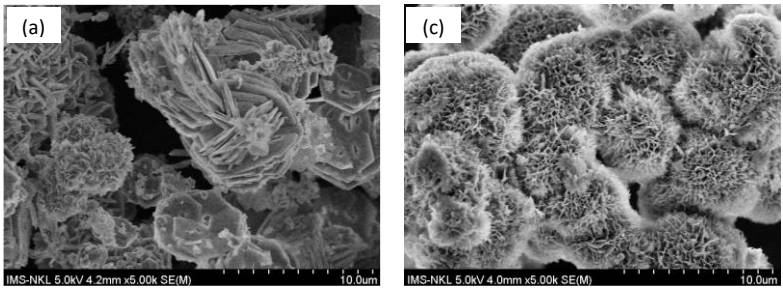

Fig. 3.18. SEM images of $MgCO_3$ (a) without surfactant and (c) with Tw80

Thanks to the small particle size, large specific surface area, medium pore size, in this thesis, the adsorption performance of some toxic gases on as-prepared nanomaterials were examined.

3.2 Adsorption of toxic gases on the obtained nanomaterials

3.2.1 Adsorption of NO_2, SO_2 gases on nFe_3O_4

Fig. 3.20a showed that after 15 minutes of exposure to NO_2 gas, the peaks on the FT-IR spectra had slight changes with the appearance of the new absorption peaks at the wavenumber near 1386 cm^{-1}. This 1386 cm^{-1} absorption peak is attributed to the vibration of the nitrate groups, NO_3^-.

The existence of NO_3^- group could be explained for the conversion of NO_2 gas adsorbed on the surface of nFe_3O_4 material into NO_3^- ions. The amount of NO_2 adsorbed reached saturation value after about 60 minutes of adsorption and was approximately equal to 108.5 mg/gFe_3O_4.

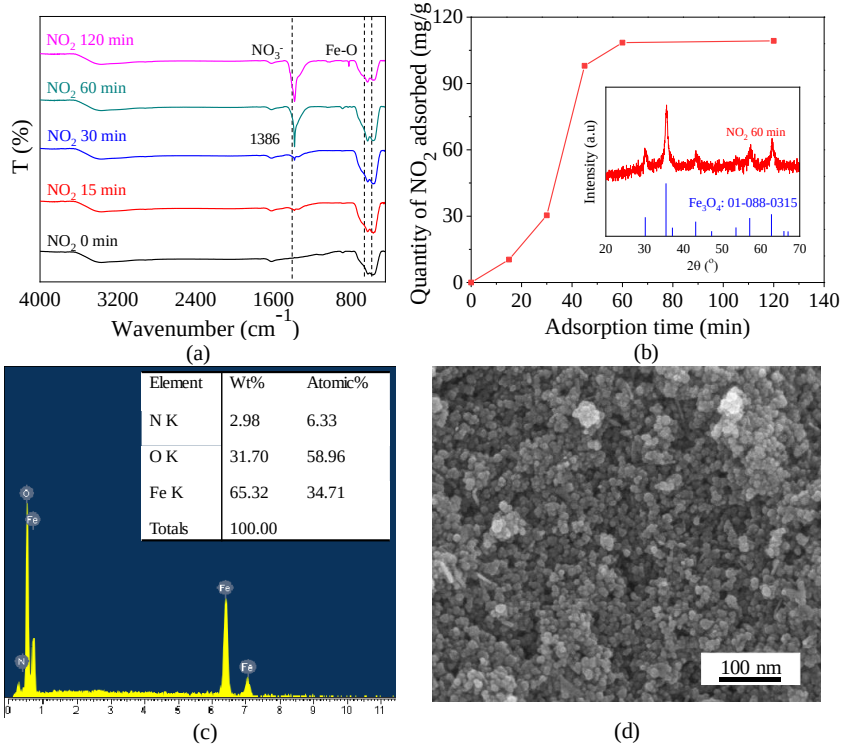

Fig. 3.20. Adsorption of NO_2 on nFe_3O_4: (a) FT-IR spectrum; (b) Amount of adsorbed NO_2 and XRD pattern; (c) EDX spectrum; (d) FE-SEM image of post-adsorption nFe_3O_4

Similar to NO_2 adsorption, the shape, size and porous structure of nFe_3O_4 after adsorption of SO_2 had no significant change. In addition, the crystal phase of the adsorbent was still consistent with the crystal structure of cubic Fe_3O_4, JCPDS 01-088-0315. In other words, the adsorption of NO_2 or SO_2 did not change the crystalline phase and porous structure of the nFe_3O_4. The steady porous structure and stable

phase state of nFe_3O_4 are criteria to be used as an adsorbent for many adsorption - desorption cycles (good regeneration and reusability).

3.2.2 Adsorption of toxic gases on nZnO and nZnO-SLS

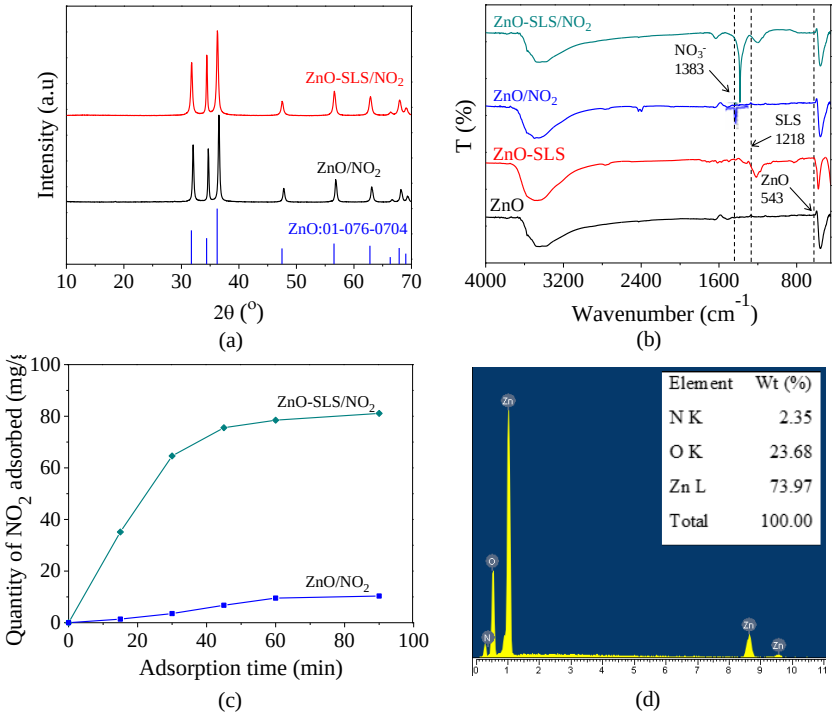

Fig. 3.22. Adsorption of NO_2 on ZnO andvà ZnO-SLS: (a) XRD patterns, (b) FT-IR spectra , (c) Amount of adsorbed NO_2, (d) EDX spectrum of post-adsorption ZnO-SLS sample

Fig. 3.22a indicated that there was no significant difference between the XRD patterns of both nZnO and nZnO-SLS samples after 90 min of NO_2 adsorption compared with the initial samples (*Fig. 3.5a*).

In contrary with XRD results, the differences could be easily seen on the FT-IR spectra (*Fig. 3.22b*) of the samples before and after NO_2 adsorption. The peak of NO_3^- at wavenumber of 1383 cm^{-1} newly appeared on the FT-IR spectrum of the post-adsorption nZnO and

especially clearly in case of the ZnO-SLS sample. The peak 1383 cm^{-1} is assigned to the vibration ν_3 of NO_3^- ions generated by the conversion of a sufficiently amount of NO_2 gas adsorbed on the surface of the adsorbent, ZnO-SLS. The gravity method exhibited the adsorption capacity of NO_2 on nZnO and nZnO-SLS was 9 and 81 mg/g. Similarly, the adsorption capacity of SO_2 on nZnO and nZnO-SLS was determined of 8.3 and 38.2 mg/g, respectively.

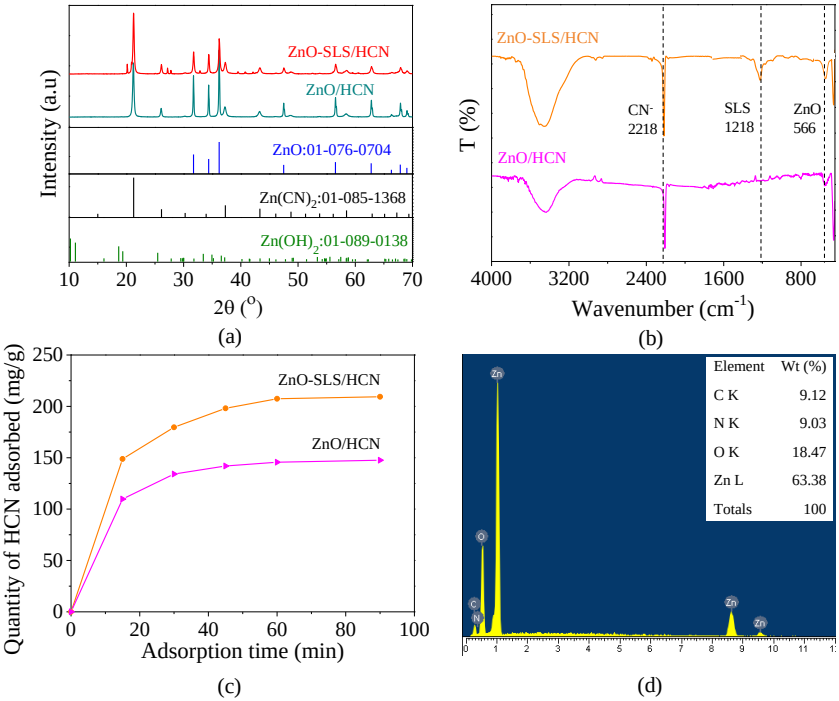

Fig. 3.24. Adsorption of HCN on ZnO and ZnO-SLS: (a) XRD patterns, (b) FT-IR spectra , (c) Amount of adsorbed NO_2, (d) EDX spectrum of post-adsorption ZnO-SLS sample

The results of HCN adsorption study showed that, on the FT-IR spectra of the post adsorption nZnO and nZnO-SLS samples (*Fig. 3.24b*), strong peaks assigned to valence vibrations $\nu_{(C\equiv N)}$ of the cyanide groups appeared at the wavenumber of about 2200 cm^{-1}. This

statement was consistent with the measurements of Spitz et al. in the study on the dissociative adsorption of HCN gas on zinc oxide powder. The adsorption of HCN gas on the nZnO-SLS led to the appearance of $Zn(CN)_2$ and $Zn(OH)_2$ crystalline phases. These newly appeared compositions may be due to the interaction between the CN^- and OH^- conjugation bases of the Brønsted acids HCN and HOH (H_2O) with the Lewis acid (Zn) sites located on the surface layer of the zinc oxide. The maximum adsorption capacity of HCN on nZnO and nZnO-SLS samples was 138 mg HCN/g and 216 mg HCN/g, respectively.

3.2.3 Adsorption of toxic gases on $nCaCO_3$-SLS

The amount of NO_2 and SO_2 gas adsorbed on $nCaCO_3$ increased very quickly during the first 90 minutes and then gradually increased to about 180 minutes of adsorption. From 180 to 480 min, the increase of quantity of adsorbed gases was negligible . The saturation capacities of NO_2 and SO_2 on $nCaCO_3$-SLS were 98 and 24 mg/g, respectively (*Fig 3.26*).

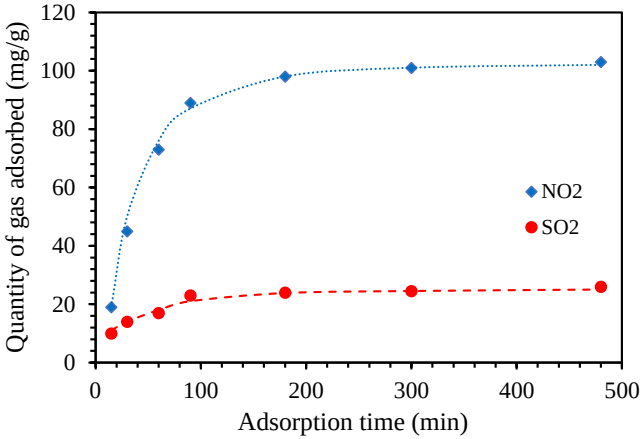

Fig. 3.26. Variation of adsorption capacities of NO_2, SO_2 on $nCaCO_3$ with time

3.2.4 Adsorption of toxic gases on $nMgCO_3$

The SO_2 adsorption process was almost saturated after about 30 minutes with the maximum capacity of approximately 114 mg/g

(*Fig. 3.33*). In the first 15 minutes, the $nMgCO_3$ material exhibited higher adsorption performance to SO_2 than to NO_2. However, from about 30 minutes onwards, when the SO_2 adsorption was almost saturated, the NO_2 adsorption continued to increase markedly. The adsorption capacity of NO_2 on $nMgCO_3$ was 125 mg/g in the first 30 minutes, and reach 230 mg/g after 180 minutes .

The results of TPR-CO analysis on the $nMgCO_3$ showed two large peaks at 357 ^oC and 586 ^oC corresponding to the CO consumption of 25.4 cm^3/g and 33 cm^3/g, respectively. Thus, $nMgCO_3$ could reduce CO concentrations generated from fires at temperatures below 600 ^oC.

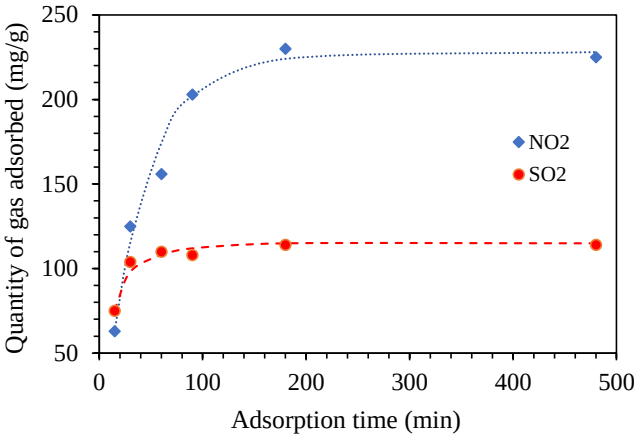

Fig. 3.33. Variation of adsorption capacities of NO_2, SO_2 on $nMgCO_3$ with time

Thus, the synthesized nanomaterials showed good adsorption performance for NO_2 and SO_2 toxic gases. The adsorption capacity of NO_2 gas was higher than of SO_2 gas on all four nanomaterials. The ZnO-based nanomaterials could adsorb HCN gas at elevated capacities. In addition to the ability to mitigate NO_2, SO_2, the $nMgCO_3$ also exhibited a promising potential in adsorption of lethal CO gas.

With the results on the adsorption efficiency as presented above, it can be seen that the inorganic nanomaterials nFe_3O_4, nZnO, $nCaCO_3$ and

$nMgCO_3$ as-prepared in this thesis are of potential adsorbents to capture toxic gases in fire incidents.

Table 3.5. Comparation of adsorption capacities of obtained nanomaterials

Adsorbent	Adsorption condition	Ads. time (min)	Saturation capatity (mg/g)		
			NO_2	SO_2	HCN
nFe_3O_4 (S_{BET} = 116 m^2/g)	- Conc. of NO_2, SO_2: 0,5% in N_2 - Humidity: 0% - Amount of adsorbent: 1 g - Gas flowrate: 200 ml/min - Temp.: 25 - 30 °C	120	108	40	–
nZnO (S_{BET} = 7,4 m^2/g)	- Conc. of NO_2, SO_2, HCN: 0,5% in N_2 - Humidity: 0%	90	9	8.3	138
nZnO-SLS (S_{BET} = 29 m^2/g)	- Amount of adsorbent: 1 g - Gas flowrate: 50 ml/min - Temp.: 25-30 °C	90	81	38	216
$nCaCO_3$-SLS (S_{BET} = 16 m^2/g)	- Conc. of NO_2, SO_2: 0,5% in N_2 - Humidity: 0% - Amount of adsorbent: 1 g - Gas flowrate: 50 ml/min - Temp.: 25 - 30 °C	180	98	24	–
$MgCO_3$-Tw80 (S_{BET} = 48 m^2/g)	- Conc. of NO_2, SO_2: 0,5% in N_2 - Humidity: 0% - Amount of adsorbent: 1 g - Gas flowrate: 50 ml/min - Temp.: 25 - 30 °C	90 180	200 230	105 114	– –

3.3 Characteristics of nano zinc borate, nZB

3.3.1 Effect of the reaction pH

When the pH was lower than 5, no precipitate appeared. At pH of 6, the amount of precipitate formed was very little, the obtained material had an amorphous structure. At pH of 7 and pH of 8, more precipitates formed. XRD patterns of samples obtained at pH of 7 and 8 showed diffraction peaks consistent with the JCPDS 01 072-3911 of zinc borate with the formula $Zn[B_3O_4(OH)_3]$ or $2ZnO.3B_2O_3.3H_2O$ *(Fig 3.38)*. The

narrow and intense diffraction peaks demonstrated that the obtained nZB materials possessed high crystallinity.

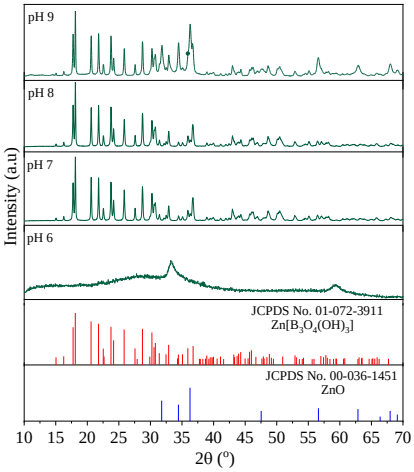

Fig. 3.38. XRD patterns of nZB at different pH

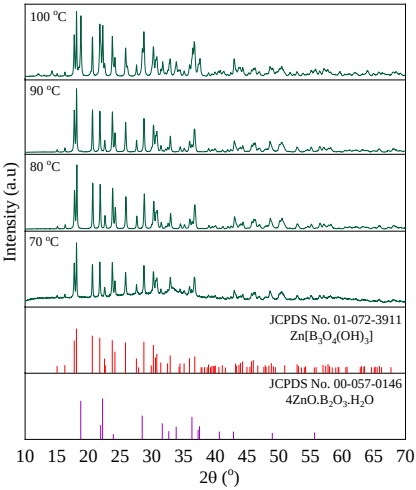

Fig. 3.40. XRD patterns of nZB at different temperatures

3.3.1 Effects of the reaction temperature

From 70 to 90 °C, all the samples had a phase composition of $Zn[B_3O_4(OH)_3]$. On the XRD pattern of the nZB prepared at 100 °C, in addition to the phase of $Zn[B_3O_4(OH)_3]$, there were also diffraction peaks of $4ZnO.B_2O_3.H_2O$ *(Fig 3.40)*. As the temperature increases, the nZB particle size drastically increased along the axes *c* and its shape changed from nanoflakes to nanorods *(Fig. 3.42)*.

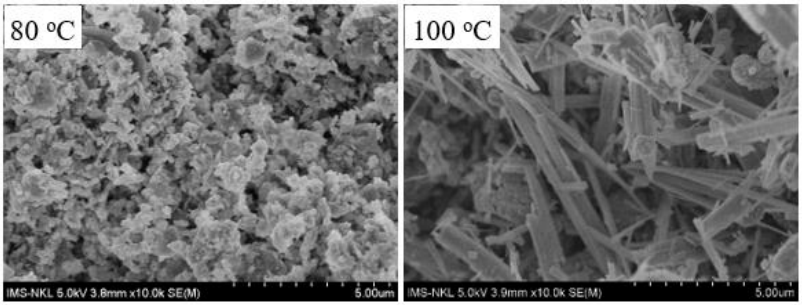

Fig. 3.42. SEM images of nZB samples prepared at 80 °C and 100 °C

3.3.3 Effect of surfactants

The XRD plots of nZB samples modified with different surfactants *(Fig. 3.43)* showed peaks consistent with the JCPDS 01 072-3911 of $Zn[B_3O_4(OH)_3]$. The sharpness of the peaks did not change significantly compared with the non-surfactant nZB sample. This indicated that PEG, OA, SLS and Tween 80 had insignificant impact on the phase composition as well as the crystallinity of the nZB.

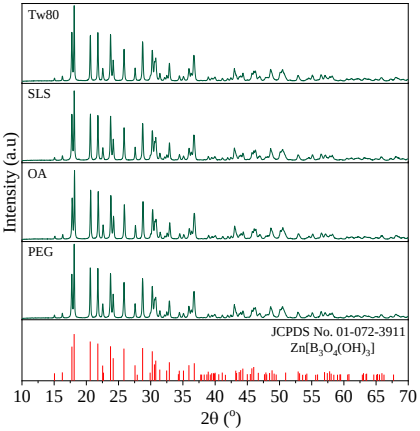

Fig. 3.43. XRD patterns of nZB modified with different surfactants

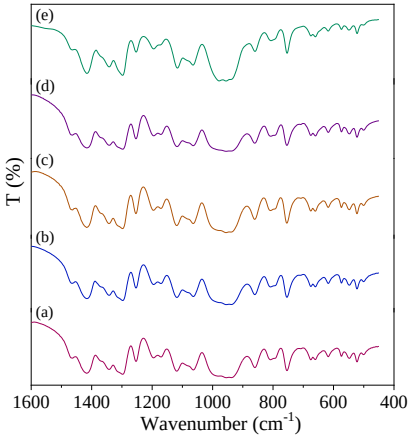

Fig. 3.44. FT-IR spectra of nZB modified with different surfactants

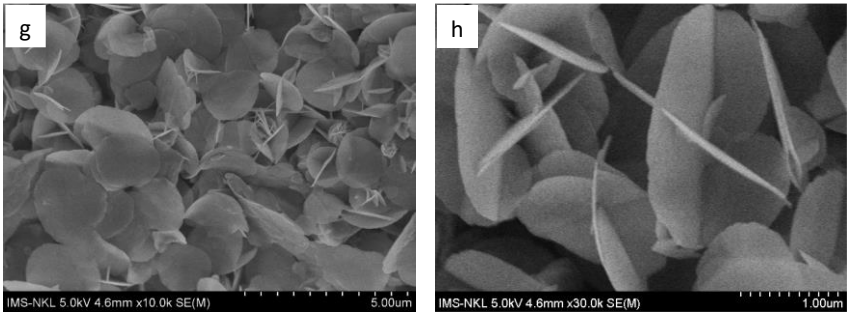

Fig. 3.45. SEM images of nZB-Tw80 sample at different magnification

The FT-IR spectra of the nZB samples synthesized in the presence of different surfactants (*Fig. 3.44*) also exhibited the absorption peaks

distinctive for the valence and bending vibrations of the functional groups in $Zn[B_3O_4(OH)_3]$. With surfactants, the nZB particles still exposed a nanoflake shape but the thickness, width and shape of the flakes changed remarkably as displayed on the SEM image (*Fig. 3.45*). In particular, nZB-Tw80 sample had a nanoflower morphology with uniform circular "petals" of approximately 20 nm thick.

Thus, pH and reaction temperature could simultaneously change the phase composition and morphology of the nZB. The surfactants had unremarkable influences on the phase composition but clear effects on the nZB morphology, forming the thinner and wider nZB particles. Favorable conditions for creating "circular petal" nZB of some micrometers in diameter and about 20 nm thick are pH of 7, reaction temperature of 80 ^oC in the presence of Tw80. This nanopetal nZB was chosen to test the synergistic flame-retardancy with other additives.

3.4 The synergistic fire-retardancy and the improvement of mechanical properties of nZB in HDPE nanocomposites

In the HDPE matrix, the nZB material exhibited better synergistic flame-retardancy with the RP/EG than with the APP/PER or MC/EG (*Table 3.7*). Nanocomposite nZB/RP/6EG/78HDPE exposed good flame-retardant performance when the nZB ratio was of 2-6% and achieved the best performance with a LOI of 26.8% and the V-0 level according to the UL94-V standard at nZB mass ratio of 6%. Besides, nZB also showed effective improvements in mechanical properties of nZB/RP/6EG/78HDPE nanocomposites. The values of tensile strength, elongation at break and impact strength of nZB/RP/6EG/78HDPE were significantly increased compared with the nZB-free HDPE composite samples. These physio-mechanical properties tended to increase as the mass ratio of nZB increased from 0 to 10% (*Table 3.8*).

Table 3.7. Flame-retardance of HDPE nanocomposites

Sample ID	UL94-V standard	Observed phenomenon, burning time	LOI (%)
HDPE	Not rated	Specimen burnt up to holding clamps with flaming drips	17.2
HDPE1	Not rated	Specimen burnt up to holding clamps, swelling, NO dripping	22.5
HDPE2	Not rated	Specimen burnt up to holding clamps, swelling, NO dripping	22.8
HDPE5	Not rated	Specimen burnt up to holding clamps, NO dripping	21.5
HDPE6	Not rated	Specimen burnt up to holding clamps, NO dripping	21.9
HDPE3	V-0	t_1 = 0.9 s, t_2 = 2.3 s, NO dripping	25.9
HDPE7	V-0	t_1 = 0.8 s, t_2 = 1.9 s, NO dripping	26.0
HDPE8	V-0	t_1 = 1.0 s, t_2 = 1.5 s, NO dripping	26.3
HDPE4	V-0	t_1 = 0,7 s, t_2 = 1.3 s, NO dripping	26.8
HDPE9	Not rated	t_1 = 1.2 s, t_2 = 32.3 s, NO dripping	24.1

Table 3.8. Effect of nZB on the mechanical properties of HDPE nanocomposites

Sample ID	Mass ratio of flame-retardants	Tensile strength (MPa)	Elongation at break (%)	Impact strength (kJ/m^2)
HDPE1	nZB/APP/PER = 0/16/6	21.76	160.22	23.46
HDPE2	nZB/APP/PER = 6/12/4	22.64	185.31	24.88
HDPE5	nZB/MC/EG = 0/16/6	20.24	117.12	9.68
HDPE6	nZB/MC/EG = 6/10/6	21.85	133.65	12.85
HDPE3	nZB/RP/EG = 0/16/6	19.15	154.78	21.82
HDPE7	nZB/RP/EG = 2/14/6	21.35	168.95	22.61
HDPE8	nZB/RP/EG = 4/12/6	21.38	177.71	22.89
HDPE4	nZB/RP/EG = 6/10/6	21.46	180.14	23.94
HDPE9	nZB/RP/EG = 10/6/6	22.06	188.94	27.12

CONCLUSIONS

1. The nFe_3O_4, nZnO, $nCaCO_3$ and $nMgCO_3$ were synthesized and the influence of surfactants on the materials has been investigated. The nFe_3O_4 was spherical particles with an average diameter of 10 nm. The nZnO and $nCaCO_3$ were nanoplates of 20 - 33 nm thick. The $nMgCO_3$ particles were flower-like spheres interlaced by nanoflakes of 10 - 15 nm thick.
2. The adsorption of NO_2, SO_2 and HCN gases by the nFe_3O_4, nZnO, $CaCO_3$ and $MgCO_3$ materials was evaluated. The nanomaterials had relatively greater capacities to adsorb NO_2 than SO_2; both nZnO and nZnO-SLS could adsorbed HCN gas effectively. The CO-TPR results showed that the $nMgCO_3$ could remove CO gas. These adsorption observations revealed the option of applying the as-prepared nanomaterials to reduce toxic gases in fire incidents.
3. The zinc borate, was synthesized from $ZnSO_4$ salt, H_3BO_3 acid and NaOH. The favorable conditions to obtain the single-phase $Zn[B_3O_4(OH)_3]$ were pH of 7 - 8, temperature range of 80 - 90 ^oC. Surfactants including OA, PEG, MD, SLS and Tw80 resulted in remarkable changes in the particle shape. The nZB-Tw80 particles' shape was like nanopetals of 1.5 - 2.5 m wide and 20 nm thick.
4. The flame-retardances of ternary combinations including nZB/APP/PER, nZB/MC/EG and nZB/RP/EG were examined in HDPE matrix. With the mass ratio of fillers/HDPE of 22/78, the nZB/RP/EG combination exhibited the best flame-retardancy. The nZB increased the tensile strength, the elongation at break and the impact strength of the nZB/RP/6EG/78HDPE nanocomposites. Overall, the 6nZB/10RP/6EG/78HDPE sample exposed the highest flame-retardancy and mechanical properties among HDPE nanocomposites.

CONTRIBUTIONS OF THE THESIS

1. In this thesis, the nanomaterials including Fe_3O_4, ZnO, $CaCO_3$, $MgCO_3$ have been tested for adsorption abilities to the toxic gases such as NO_2, SO_2, HCN và CO. The nanomaterials showed good adsorption capacities and might be used in the removal of toxic gases emitted from unwanted fires.

2. In this thesis, the influencing factors on the precipitation reaction of nano zinc borate including pH, temperature and surfactants have been systematically investigated. The appropriate conditions for the synthesis of nanopetal $Zn[B_3O_4(OH)_3]$ were found at the pH range of 7 to 8, temperature range from 80 to 90 ^oC in the presence of Tween 80 surfactant.

3. In this thesis, nZB/RP/EG/HDPE flame-retardant nanocomposites have been successfully fabricated from the mixtures of as synthesized nanopetal $Zn[B_3O_4(OH)_3]$, red phosphorus and expanded graphite in HDPE matrix. The nZB/RP/EG systems had good synergistic effects. The nZB/RP/EG/HDPE nanocomposites possessed LOI higher than 26% and reached the V-0 level of UL94-V standard with mass ratios of 6% EG, 78% HDPE, 2 - 6% nZB. The most appropriate mass ratio of nZB was 6%.

LIST OF THE PUBLICATIONS RELATED TO THE DISSERTATION

1. Xuan Manh Pham, Duy Linh Pham, **Nguyen Thi Hanh**, Tuyet Anh Dang Thi, Le Nhat Thuy Giang, Hoang Thi Phuong, Nguyen Tuan Anh, Hac Thi Nhung, Giang Truong Le, Mai Ha Hoang, and Tuyen Van Nguyen. *An initial evaluation on the adsorption of SO_2 and NO_2 over porous Fe_3O_4 nanoparticles synthesized by facile scalable method*. Hindawi Journal of Chemistry **(2019)**.
2. **Nguyen Thi Hanh**, Dang Thi Tuyet Anh, Le Nhat Thuy Giang, Hoang Thi Phuong, Nguyen Tuan Anh, Hoang Mai Ha, Nguyen Van Tuyen. *Synthesis of $CaCO_3$ nanoparticles using surfactants for adsorption of SO_2 and NO_x gases*. Vietnam J. Chem 57(4E1,2) **(2019)** 406-410.
3. **Thi Hanh Nguyen**, Xuan Manh Pham, Thanh Nhan Nguyen, Nhung Hac Thi, Tuyet Anh Dang Thi, Quang Vinh Tran, Anh Tuan Vu, Mai Ha Hoang, Tuyen Van Nguyen. *Preparation of ZnO nanoflakes and assessment of their removal of HCN, NO_2 and SO_2 toxic gases*. International Journal of Materials Research 112, no. 1 **(2021)**:10-16.
4. Truong Cong Doanh, Hac Thi Nhung, **Nguyen Thi Hanh**, Nguyen Thi Thu Hien, Doan Tien Dat, Vu Minh Tan, Hoang Mai Ha. *Synthesis of nanoplatelet zinc borate and its combination with expandable graphite and red phosphorus as flame retardants for polypropylene.* VNU Journal of Science: Natural Sciences and Technology 38(3) **(2022)** 86-96.